Nanoscale

Single- and Bi-Exciton Character in Ligand-Modified Silicon Nanoparticles as Demonstrated via Single Particle Photon Statistics and Plasmonic Effects

Journal:	*Nanoscale*
Manuscript ID	NR-ART-01-2021-000108.R1
Article Type:	Paper
Date Submitted by the Author:	12-May-2021
Complete List of Authors:	So, Woong Young; National Cancer Institute, Laboratory of Cell Biology Abbas, Sikandar; Carnegie Mellon University, Chemistry; Lahore University of Management Sciences, Li, Qi; Stanford University, ; Carnegie Mellon University, Jin, Rongchao; Carnegie Mellon University, Chemistry Peteanu, Linda; Carnegie Mellon Univ, Chemistry; Carnegie Mellon University

6/3/2021

Single and Bi-excitonic Characteristics of Ligand-modified Silicon Nanoparticles as Demonstrated *via* Single Particle Photon Statistics and Plasmonic Effects

Woong Young So, Sikandar Abbas, Qi Li, Rongchao Jin, and Linda A. Peteanu*
Department of Chemistry, Carnegie Mellon University, Pittsburgh, PA, USA 15213

Abstract

Silicon nanoparticles (Si NPs) are of great interest to researchers due to their fluorescence properties, low toxicity, and the low cost of the Si precursor. Recent studies have shown that Si NPs surface-modified with secondary aryl amine ligands emit light at wavelengths ranging from cyan to yellow and with quantum yields of up to 90%. The predominant emitting state in these species has been assigned to a charge-transfer (CT) transition from the ligand to the Si particle as the emission wavelength is determined by the dipolar properties of the ligand rather than the size of the Si core. This contribution focuses on the single-molecule emission properties of Si NPs functionalized with a 1,2,3,4-tetrahydrocarbazole-4-one ligand (Te-On) which have a peak emission wavelength of 550 nm and a quantum yield of 90%. In single-particle dispersed emission spectra, a weak long-wavelength sideband is seen in addition to the dominant yellow emission derived from the CT state. The photon statistical behavior of single Si NPs in the red emission region is consistent with that of a state having collective or bi-excitonic character. In contrast, the yellow emission exhibits predominantly CT character. Deposition of the sample onto a thin gold film causes the CT emission to be quenched whereas that attributed to a bi-exciton state of the Si core is enhanced. These results provide new insights into the mechanism of single-molecule intensity fluctuation in these surface-modified silicon nanoparticles that will benefit proposed applications in biological labeling and as single-photon sources.

*peteanu@cmu.edu.

Electronic Supporting Information (ESI) is available.

Introduction

Following the first observation of bright photoluminescence from nanoporous Si,[1,2] a key goal in this field has been to design and produce nanostructures with brighter and wavelength-tunable emission. Due to the relatively high abundance of Si and its low toxicity, silicon nanoparticles (Si NPs) are considered promising alternatives to the more extensively studied heavy-metal-containing quantum dots for a variety of biological and opto-electronic applications.[3] Because these materials are biodegradable in the kidney without toxicity, they are also viable for *in vivo* applications.[4,5] These desirable properties have motivated extensive research into the development of free-standing Si NPs. Several distinct types have been reported that exhibit a rich variety of emission properties and mechanisms.[6] One general class, ligand-free particles and those surface passivated with hydrogen atoms or aliphatic hydrocarbons, exhibit red or near-infrared emission from the Si core that is wavelength tunable *via* quantum confinement.[7–10] In contrast, Si NPs functionalized with aromatic secondary amine ligands exhibit bluer emission arising from a ligand to Si charge-transfer (CT) state.[11–14] Functionalization with aliphatic amines can produce emission with characteristics of either the core or surface states.[15–20]

This contribution is a detailed examination of the dispersed emission spectra and photon statistics of single Si NPs surface functionalized with the aromatic secondary amine ligand 1,2,3,4-tetrahydrocarbazole-4-one (Te-On, Chart 1). This particular system was chosen because it has a high emission quantum yield making it suitable for single-molecule (SM) spectroscopy. These combined methods unambiguously show that each particle exhibits characteristics of both single quantum levels and collective states with the former dominating the emission. The relative intensity of these two types of emission is altered if a plasmonic surface is in proximity to the Si NPs, as has been previously observed in semiconductor quantum dots (QDs).[21–25] This work is placed into context of recent studies of the emission mechanism in other Si NP systems.

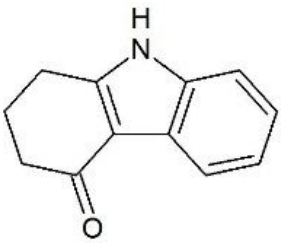

Chart 1. Structure of 1,2,3,4-tetrahydrocarbazole-4-one (Te-On)

Experimental

The yellow emitting Te-On Si NPs were synthesized using the previously published methodology.[12] Silicon tetrabromide, glyme, sodium, and naphthalene were purchased from Sigma-Aldrich. 1,2,3,4-tetrahydrocarbazole-4-one was purchased from TCI America. Acetonitrile was purchased from Fisher Scientific. The absorption spectra were recorded using Agilent Cary 50 Bio UV/Vis spectrometer. The fluorescence spectra were recorded on Jobin-Yvon FluoroMax 2. Characterization of the samples prepared by this method by FTIR and TEM has been published previously.[11,12] The TEM results[12,14] (ESI Figure S1) indicate that the NPs are 2.63 ±0.8nm..

For single-particle studies, the Te-On Si NPs were diluted to pM concentrations. For time trajectory and anti-bunching studies in the solid state, these NPs were mixed with a polymer matrix (PMMA solution of 2 wt. % in acetonitrile (MeCN)). The sample solution was then spin-coated at 4000 rpm for 30s (Laurell WS-650MZ-23NPP). The thin Au films were prepared by sputter coating the metal film onto cleaned glass coverslips. The deposition occurred under inert Ar conditions at 0.06mbar (or 31mA) and 1kV applied potential resulting in a sputtering rate of 0.4nm/s. The total deposition time was 5s to yield a 2nm thick Au film. The slide on which the 2nm layer of gold was sputtered was then directly attached to the top surface of Si NP/PMMA film (~50nm) before the PMMA layer hardened. A sample with a non-Au-coated coverslip was created for a control.

Dispersed emission spectra of single Si NPs were obtained using a home-built system based on total internal reflection (TIRF) illumination and CCD detection.[26,27] TIRF microscopy was performed using through-objective excitation *via* a 60x 1.4 NA oil immersion objective on an inverted microscope (Olympus IX-71). The excitation source was the 488 nm output of an Ar-Kr laser (Coherent). The spectra from single yellow Si NPs were collected using a CCD camera (Photometrics Evolve 512 EMCCD) having 11μm^2 pixels. A mechanical slit was placed in the emission path to isolate the emission of individual Si NPs followed by a 495 nm long pass filter to

remove scatter. Next, a 300g/mm transmission grating (Thorlabs GT13-03) was placed to disperse the emission light from individual Si NPs which was coupled through a lens relay system onto the CCD. Using a 100mm focusing lens placed before the CCD, a spectral range of 300nm was obtained based on an inverse linear dispersion of 33nm/mm (0.215nm/pixel).

For single-particle confocal microscopy, the excitation source was a 485 nm pulsed diode laser (Picoquant). A 1.4 NA 100x oil objective (Olympus UPlanSAPO 100x 1.4 oil) was mounted on an inverted microscope (Olympus IX-71). The emission was directed through a 100-μm pinhole to a 50:50 beam splitter (Semrock) which split the emission onto two single photon avalanche diodes (Micro Photon Devices PDM50) in a Hanbury-Brown-Twiss geometry. Filters of 540nm ± 25nm, 605nm ± 27.5nm, and 650nm ± 20nm (all from Thorlabs) were used. Time-tagging of the photons was performed using the PicoHarp 300 and PHR 800 electronics (Picoquant). All the data (photon bursts, anti-bunching, and fluorescence correlation) were collected and analyzed using the SymPhoTime software package (Picoquant). Excitation powers of 25-140μW were used as measured before the beam entered the microscope. This corresponds to 2.5-14μW on the sample or a maximum power density of ~10kW/cm^2 assuming a focused beam radius of ~211 nm (see ESI for calculation). With a pulse repetition rate of 10MHz and assuming an extinction coefficient at the excitation wavelength of 1.2 x 10^5 (2.4 x 10^{-16} cm^2), this gives an average number of excitations per pulse (<N>) of 0.5 at the minimum power required to observe the red emission which is 7kW/cm^2 (see ESI for calculation).[28]

Results and Discussion

The bulk absorption and emission spectra of Te-On Si NPs are reproduced in Figure 1a. A reduction in the inhomogeneous linewidth is obtained by dispersing the emission of single Si NPs which are deposited on the cover glass after spin-coating the solution of Si NPs with PMMA in MeCN (Figure 1b and ESI Figure S2).

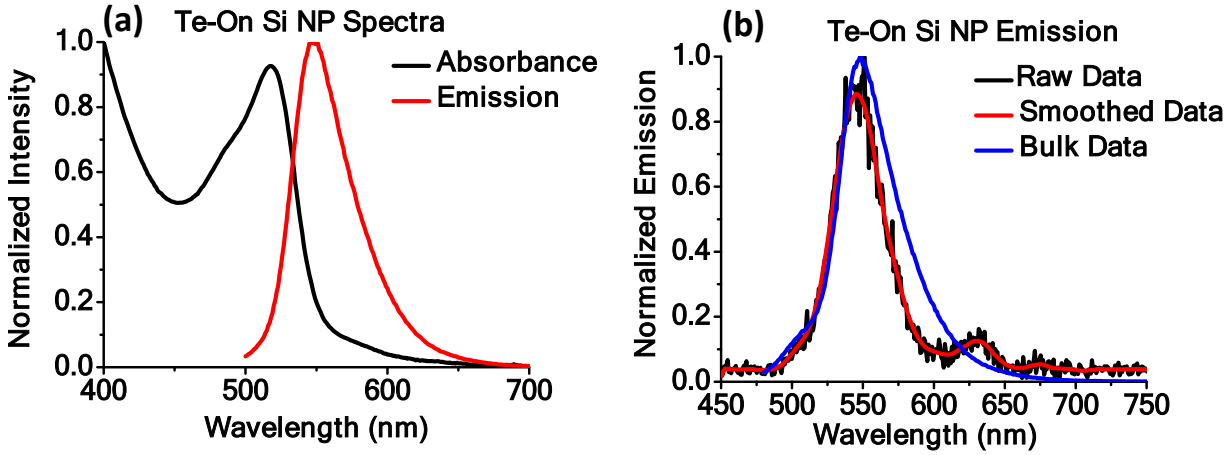

Figure 1 (a) Normalized absorbance and emission of bulk Te-On Si NP in water and (b) single-particle dispersed emission spectra of Te-On Si NP deposited onto cover glass.

The single particle spectrum contains a weak satellite band at 625nm (red band) that is 270meV lower in energy than the predominant emission at 550nm. A survey of the literature indicates that a band ~180meV lower in energy than the main emission peak (yellow band) and in this wavelength region is common to Si NPs that are formed by very different synthetic routes though the relative intensity of two bands is highly sample-dependent.[29–33] For example, a peak in approximately this wavelength region was observed in single-particle dispersed emission measurements on organic-monolayer-coated Si NPs by Barbara and coworkers and more recently by Kůsová *et al.* in Si NPs functionalized with xylene ligands by the combination of electrochemical etching and ligand passivation.[29–31] In both cases, however, its intensity relative to that of the higher-energy emission band is significantly larger than that observed here.

The assignment of this low-energy band has been somewhat controversial. It has been attributed to a vibronic transition in a surface oxide state (Si=O or Si-O-Si) by Borczyskowski,[32] Buratto,[33] and Korgel[29] due to the similarity of the 180meV spacing to the expected frequency of the Si-O vibration. More recently, Kůsová *et al.* assigned this signal to the splitting of energy levels in the core of quantum-confined Si nanocrystals associated with the formation of trions.[30,31] As unmodified Si emits in the red and near-IR,[16,19] this emission is plausibly associated with the Si core. Next we show that emission in the red region shows very distinct photon statistics from that

of the dominant emission peak and that this can be used to unambiguously assign these bands to emission arising from collective *versus* single particle states, respectively.

Confocal microscopy of single Si NPs in water was performed by monitoring emission bursts at wavelengths corresponding to the band maximum (540nm ± 25nm) and to the red sideband region (650nm ± 20nm) by splitting the total emission onto two separate photodiode detectors (Figure 2a and b) in a Hanbury Brown-Twiss[34–36] configuration. The signal in the red is notably weaker, consistent with the appearance of the dispersed emission spectrum (Figure 1b). Figure 2c shows that the bursts in these two wavelength regions coincide when a single Si NP passes through the focal point which shows that they originate from the same particle. The emission lifetimes of the samples were recorded under a variety of conditions (Figure 2d and Table 1).

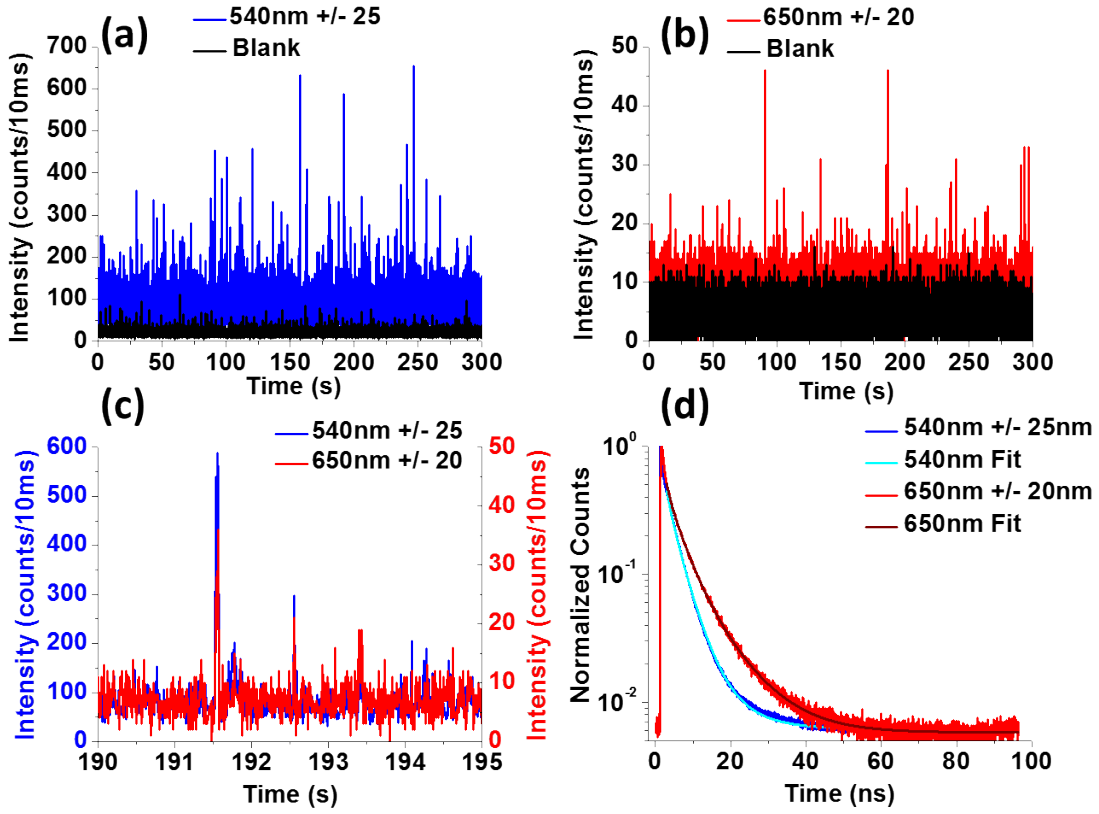

Figure 2. Solution-phase burst measured from Te-On Si NPs collected simultaneously at the (a) emission maximum (540nm) and (b) red emission region (650nm) compared to the blank solution. (c) Expanded temporal scale showing coincidence of bursts measured at 540nm and 650nm. (d) Emission lifetimes measured at the emission maximum and in the red emission region.

In solution, the red and yellow emissions exhibit similar decay components albeit with very different weights. Specifically, the dominant component of both is essentially that reported for the bulk sample (~3ns)[12] though the amplitude of the ~10 ns component is significantly greater in the red than in the yellow (Figure 2d and Table 1). Proposed interpretations of the various emission decay components are discussed later.

Table 1: Lifetimes and normalized $g^{(2)}(0)$ values for Si NPs in absence and presence of gold substrates

Sample	$\tau_1{}^a$ ($a_1{}^b$)	τ_2 (a_2)	τ_3(a_3)	$g^{(2)}(0)$
Bulk Solution	3.0 [c]			
SM[d] Solution 540nm	1.3 (.23)	3.8 (0.72)	9.2 (0.05)	0.28
SM Solution 650nm	1.2 (0.17)	3.9 (0.58)	9.7 (0.25)	0.81
SM PMMA/glass 540nm[e]	1.0 (0.13)	3.7 (0.50)	9.8 (0.37)	0.26
SM PMMA/glass bright state[f]		3.4 (0.52)	9.5 (0.48)	0.05
SM PMMA/glass interm. state[f]	1.0 (0.08)	3.2 (0.32)	9.5 (0.60)	
SM PMMA/glass dim state[f]	1.1 (0.3)	3.1 (0.33)	9.6 (0.37)	0.7
SM PMMA/Au 540nm	IRF Limited (~70%)	2.6 (0.58)[g]	8.5 (0.42) [g]	0.7

SM PMMA/Au bright state		2.7 (0.41)	8.5 (0.59)	0.24
SM PMMA/Au dim state	IRF Limited (~95%)	2.6 (0.62) [g]	8.7 (0.38) [g]	0.82

[a] in nsec, [b] relative amplitude, [c] ref 12 [d] single molecule, [e] collected without intensity thresholds (see text), [f] collected with intensity thresholds (see text). [g] obtained by tail fitting

Fluorescence correlation spectroscopy (FCS) was performed separately on emission collected from the red and yellow spectral windows in order to verify that the sample concentration used was in single molecule regime (*i.e.* the average number of emitters in the focal volume is less than unity, Figure S3a in the ESI). Moreover, the shape of the FCS curves measured for the red and yellow emissions are indistinguishable and the radius computed from the diffusion constant is consistent with that expected for a single Si NP (Figure S3b in the ESI). These points are critical for the proper interpretation of the fluorescence anti-bunching measurements described below.

Photon anti-bunching measurements[37] are frequently used to validate that emission derives from a single species rather than from a collection of uncoupled emitters.[38–40] Recently, this method has also been used to identify bi-excitonic emission in inorganic QDs.[21,35,41] It involves measuring the second-order cross correlation function $g^{(2)}(\tau)$ of the emitted photons which is defined as

$$g^{(2)}(\tau) = \frac{< I_1(t) I_2(t+\tau) >}{< I_1(t) >< I_2(t+\tau) >} \qquad (2)$$

where $I_1(t)$ and $I_2(t)$ are the signal intensities of the two channels and the brackets denote expectation values. The second order correlation function here compares the fluorescence intensity at time t with that after a time delay, τ. For simple emitters, such as dyes, only one photon can be emitted at time $\tau = 0$ because the system must recover to the ground state before a second photon is emitted. There will therefore be a dip at the amplitude of the center ($g^{(2)}(0)$) peak that is referred to as anti-bunching. However, if a peak is observed at zero time, this means that two or more photons have been detected simultaneously (within a single laser pulse). This may be the

case if, for example, there is more than one emitter in the focal volume, if emission derives from an aggregate, or if more than one photon is emitted simultaneously upon excitation. The latter would be the case for a bi-excitonic state.[35,42] Single dye molecules generally show strong anti-bunching (negligible $g^{(2)}(0)$ peak)[43–46] and many inorganic QDs also exhibit this phenomenon at low excitation powers. For example, strong anti-bunching behavior in semiconducting QDs was reported several years ago by the groups of Buratto and Moerner.[34,36] More recently, Bawendi and coworkers performed these measurements using pulsed excitation to quantify the relative yields of single- and bi-excitonic states in these species.[34–36,47] Briefly, these authors showed that, while anoparticles such as CdSe exhibit strong anti-bunching in the low power limit, the size of the $g^{(2)}(0)$ peak increases significantly with laser power.[36,47,48] They developed a framework to associate the ratio of the size of the $g^{(2)}(0)$ peak to the sideband peaks (appearing at $\pm t_{rep}$ where t_{rep} is the laser repetition rate) with the probability of forming a bi-excitonic state in the nanoparticles. Whereas this analysis is appropriate for a small number of excitons, <N>, Moyer and coworkers developed a method appropriate for large <N>.[21]

Though both the yellow and red emission bands of Te-On Si NPs originate from the same particle, they show quite different photon intermittency and anti-bunching characteristics as described next. This behavior is used to critically examine some possible assignments of the physical origin of these two bands in the context of the broader literature on Si NPs and of analogous measurements on semi-conducting QDs. The values of $g^{(2)}(\tau)$ for photon emission were measured in three wavelength regions: the emission maximum (540nm ± 25nm), an intermediate region (605nm ± 27.5nm), and in the red (650nm ± 20nm). Figure 3 shows that the value of $g^{(2)}(0)$ is small at the emission peak and increases significantly as the collection wavelength increases. No signal is observed from the blank solution (ESI Figure S4) meaning that any contribution of scatter or Raman to $g^{(2)}(0)$ can be neglected.

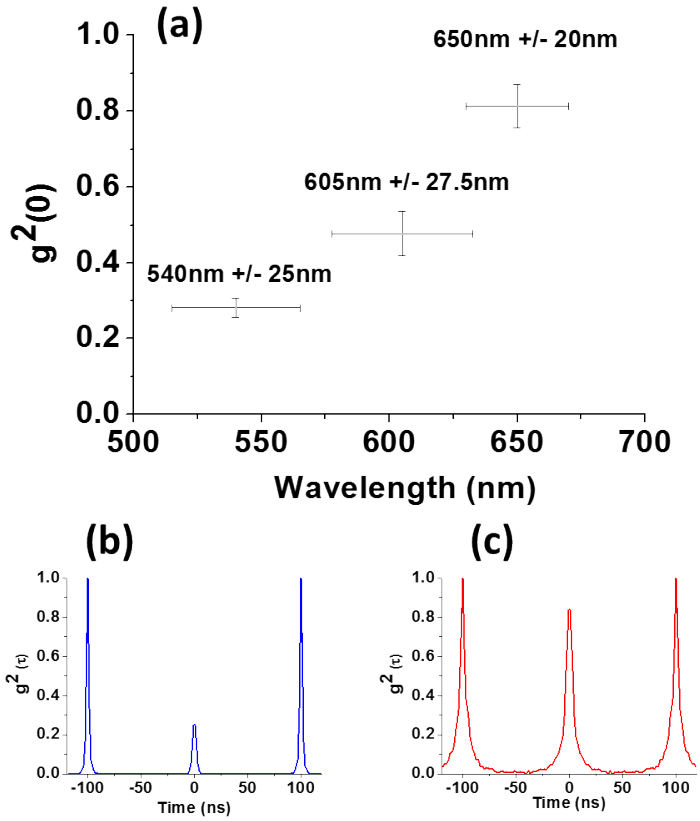

Figure 3. (a) Magnitude of $g^{(2)}(0)$ measured for Te-ON Si NPs in water at 540nm ± 25nm, 605nm ±27.5nm, and 650nm ± 20nm. (30 measurements each). Anti-bunching signal measured at (b) 540nm ± 25nm and (c) at 650nm ± 20nm.

The small value (0.2) of $g^{(2)}(0)$ measured at 540nm is above that expected for a pure single quantum system which is zero. This is likely due to spectral overlap between the yellow and red emission bands evident in the single Si NP emission spectra (Figure 1b) and the solid-state data presented below. Whereas the overall emission is linear in power over the range reported, distinctly different and sub-linear power dependences of the $g^{(2)}(0)$ signals from the yellow and red emission regions are observed (ESI Figure S5).

Next, the photon statistical behavior of single Si NPs within PMMA films was investigated. A sample time trajectory study of a single Si NP (Figure 4a) shows large photon bursts on a more continuous background that is distinct from the dark count level of the camera (Figure 4a). We designate these two emission types as 'bright' (above 80 counts/10ms) and 'dim' (0-80

counts/10ms), respectively. This dim state is effectively the 'off' state for these blinking NPs as the signal from these systems never completely drops to the dark count level. The emission lifetimes of the bright and dim states were measured separately by setting the detection threshold appropriately. Both states exhibit non-single-exponential decays (Figure 4b and Table 1) that can be fit using decay components similar to those measured in solution but with very different weightings. In addition, ~30% of the decay of the dim component occurs within the instrument response function of ~200ps (IRF, Figure S6 in the ESI). The assignments of these emission decays will be discussed later.

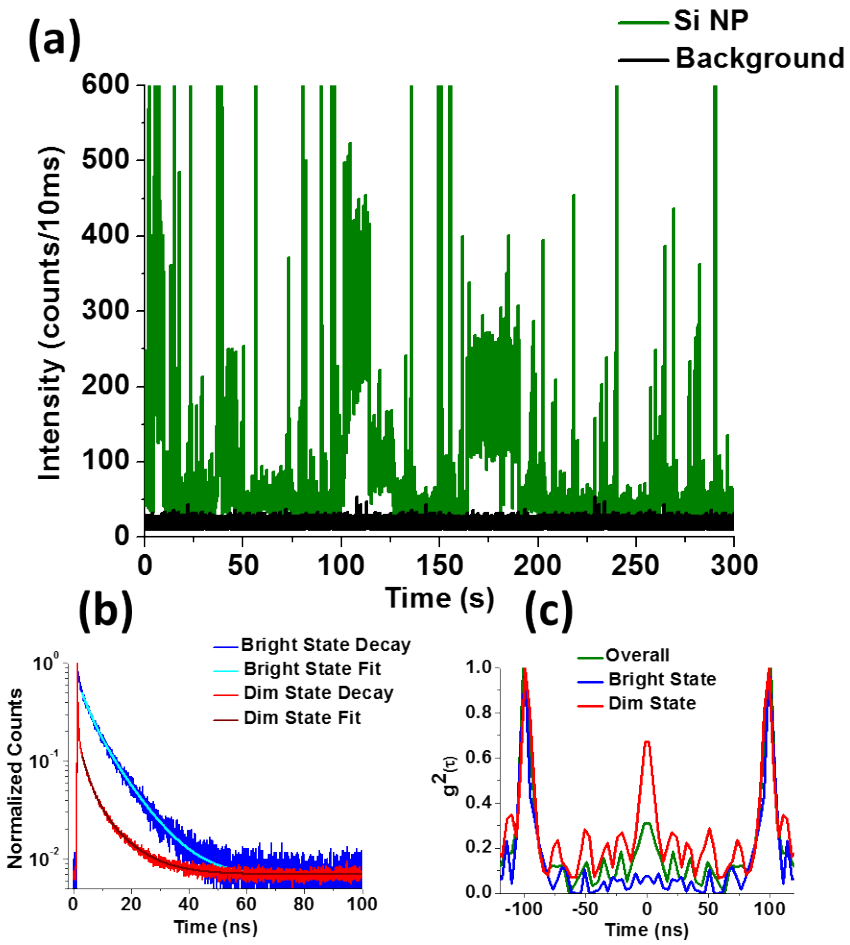

Figure 4. (a) Time trajectory of a single Ti-On Si NP in PMMA collected over 300 seconds, (b) comparison of emission decays of the bright and dim states (see text), and (c) comparison of anti-bunching obtained for various emission thresholding levels (see text). Data collected at 540nm ± 25nm.

Anti-bunching measurements were performed by collecting all the emitted photons (bright and dim) and then setting a collection threshold to separate the bright and dim emitting states as described above. An emission bandpass filter with a transmission wavelength range of 515nm – 565nm was used to capture the spectral region corresponding to the strong emission peak (Figure 1b). The value of $g^{(2)}(0)$ for the combined bright and dim emission was 0.2. However, by measuring the value of $g^{(2)}(0)$ for the bright and dim states individually (Figure 4c), we see the former exhibits essentially complete anti-bunching while the opposite is seen for the dim state (Table 1). These measurements are consistent with the significant 'blinking' observed in the time traces of the bright state and low degree of intermittency in the time trace of the dim state (Figure 4a). The non-zero $g^{(2)}(0)$ value measured for photons collected within the main emission band if no thresholding is applied is due to the spectral overlap between the red emission peak and the main emission band of the CT state (Figure 1b).

To summarize the findings thus far, despite the fact that both yellow (bright) and red (dim) emission arise from the same particle, the former exhibits the properties expected of a single quantum system whereas the latter behaves like a collection of emitters (*i.e.* a collective state) or, in other words, as a system that can emit more than one photon simultaneously. The single-quantum-level characteristics of the bright yellow emission is somewhat surprising given that it likely contains contributions from numerous bound ligands and potentially from surface and core states of the Si particle.[12] Nonetheless, similar behavior has been observed in numerous multi-chromophore organic emitters and inorganic QDs,[34–36,47] though the underlying mechanisms differ. It bears noting that similar photon statistics would be expected for this general class of Si NPs, meaning those with conjugated surface ligands, as they have similar electronic properties[14] and show broad emission in the red.[11,12,17]

Turning to the assignment of the dim red-emitting state, we examine several possibilities suggested by the literature and by the results presented thus far. Signal from aggregates containing more than one Si NP is unlikely to be the source of the non-zero $g^{(2)}(0)$ values as the red and yellow emission in dilute solution arises from the identical particle and the yellow emission exhibits clear anti-bunching, as discussed earlier. Moreover, the FCS data (ESI Figure S3) give no evidence for

aggregation. Nonetheless, aggregates or other states that can emit more than one photon and that can reside on a single particle must still be considered. One possibility is that the red emission is associated with dimers or higher-order aggregates of the Te-On ligand. In ref. 12 the emission spectrum of Te-On Si NPs formed by the addition of excess ligand is shown to be red shifted to 555 nm from the value at lower loadings (546 nm). If the aggregated ligands still behave like a collection of independent emitters, a non-zero $g^{(2)}(0)$ value would be expected. The scenario is unlikely, however, as energy transfer between closely packed organic molecules is typically fast and leads either to emission quenching and a reduced lifetime or to emission from a single lowest-energy state and a $g^{(2)}(0)$ close to zero.[49]

We next considered whether a species other than the organic ligands present in Te-On Si NP could contribute to multiple photon emission given that the ligand only comprises ~10% of the bonds on the surface.[12] The unmodified particle, which contains Si-Br bonds as well Si-O-H and O-Si-O bonds due to oxidation, absorbs at 400 nm. Its emission spectrum is broad and very weak with a peak at 420 nm.[12] Our efforts to measure its SM properties were unsuccessful due to the weak signal and its poor stability. However it may be a contributing factor given that there are reports in the literature of Si NP emission in the spectral range reported here and with ns lifetimes arising from partially-oxidized surface states.[50,51] Unfortunately, to our knowledge, the anti-bunching characteristics of these species have not yet been reported.

The mechanisms considered thus far would reduce the contrast (*i.e.* increase $g^{(2)}(0)$) through excitation of multiple uncorrelated emitting states such as multiple species within a single particle. We next examine possible contributions from more than one absorption event within a single laser pulse to create two CT states. Support for this mechanism would be observing an increase of $g^{(2)}(0)$ with laser power. Unfortunately, due to the weak signal in the red spectral region, this dependence could not be measured as the signal at lower laser powers was not sufficient to measure anti-bunching. Nonetheless, the probability of exciting two CT transitions can be estimated as follows. The number of excited states created per pulse is ~0.5 (see ESI) using an estimated absorption coefficient at 485 nm of 1.7×10^5 and the minimum laser powers required to see the red emission with adequate signal to noise (10μW at the sample at 10MHz laser repetition rate).[28,52]

Using this value, the Poisson distribution gives a 30% probability of absorbing a single photon and a 8% probability of absorbing two (see ESI for calculation). In principle, absorption of two photons can generate CT states on two separate (non-aggregated) ligands on the Si NP surface or a doubly-excited CT state assuming similar extinction coefficients and energy gaps for both transitions. If the quantum yields of the two emitting states are presumed to be equal, the ratio 0.08/0.3 or 0.27 will be equal to the ratio of the areas under the red sideband and the main emission band of the SM spectrum (Figure 1b). Calculation of this ratio involves numerous approximations which may explain why it is larger than the experimental value of ~ 0.1. However, this model would imply that the formation of two excited CT states or a doubly-excited state lowers the transition energy rather than raises it as would be expected from the increased Coulombic repulsion. Alternatively, these states may be formed primarily in aggregated ligands causing them to have lower bandgaps than those formed on non-aggregated ligands.[12] In this case, we would expect the red emission to decay more rapidly than the yellow emission because multiply-excited states are typically shorter lived than the corresponding singly-excited state due to the potential for annihilation or enhancement of other non-radiative processes and/or a decrease in the radiative lifetime.[53] However, in solution, the reverse is true (Table 1 and Figure 2d).

Thus far we have argued that the characteristics of the red emission are not fully consistent with assignment to excitation of more than one CT state, a CT state on aggregated ligands, or of other surface states. Finally, we consider the possibility that the red emission arises from the Si core itself or from a process involving interaction of the core and a surface state.[30,31] The red band of Te-On Si NPs lies in spectral region expected for Si core emission though its lifetime (Table 1) is shorter than that previously reported in other Si NPs.[54] Its low intensity (Figure 1b) suggests that its fast decay is predominantly non-radiative. There is some literature support for our proposal that this emission arises from a bi-exciton state of the core. Specifically, Si nanocrystals prepared by plasma etching and electron-beam lithography (which emit from the nanoparticle core) show a ns emission decay component at high fluences due to non-radiative Auger recombination of the bi-exciton state.[53] The longer decay components (>100ns) reported for these Si nanocrystals and assigned to the exciton state would be unobservable at the repetition rate of our laser system.

In summary, bi-excitonic character in the core emission of various preparations of Si nanocrystals has been identified as a decrease in the excited state lifetime with excitation power.[53,55] Unfortunately, because the red emission could not be observed below saturation power levels, we were unable to monitor this evolution from single to bi-excitonic character with increased laser power either as decrease in the lifetime or an increase in the value of $g^{(2)}(0)$. However, as described next, the effects of a nearby plasmonic surface on the size of the $g^{(2)}(0)$ peak and on the relative intensities of the bright and dim emission bands is also consistent with our assignment of the latter to a bi-excitonic state of the core.

Numerous studies on semiconductor QDs situated close to plasmonic surfaces have reported an enhancement of the bi-excitonic emission and a quenching of the single exciton emission.[21,22,24,25,48,56–58] For a recent review see ref. 23. Here, coupling of the Si NPs to the surface plasmon resonance (SPR) of Au was found to modify their excited state dynamics and emission properties in a similar fashion. Figure 5 shows the spectral overlap between the Si NPs in PMMA and the plasmon band of the gold film onto which they were deposited. The emission time traces and photon distributions (Figure 6) demonstrate quenching of the 'bright' emission (defined as >100 counts/10ms) and a 63% increase in the 'dim' emission level (65 counts/10ms *versus* 40 counts/10ms) on the gold surface *versus* that on uncoated glass.

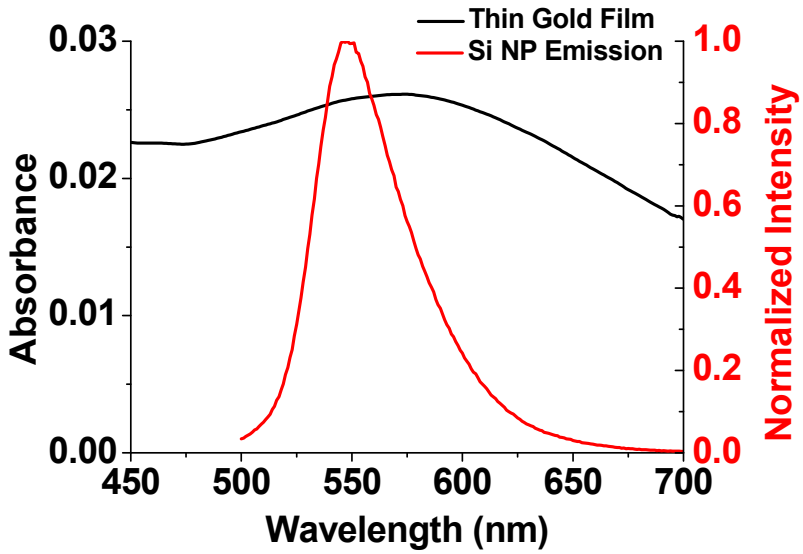

Figure 5. Surface plasmon resonance of the thin gold film substrate shown overlaid with the emission of the Si NPs.

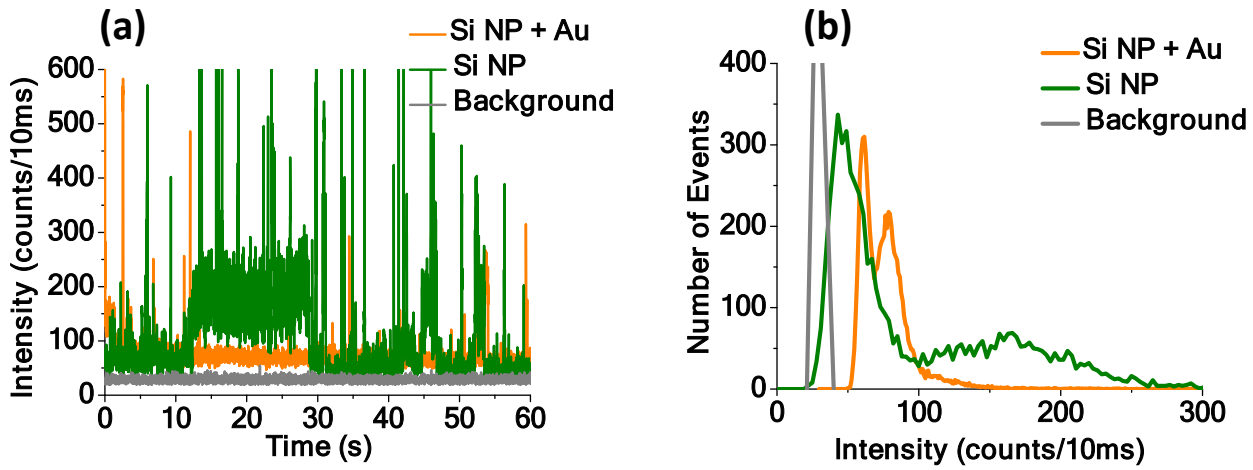

Figure 6. (a) Time trace of Si NP + Au film (yellow), Si NP on glass (green), and background (grey). (b) Intensity distributions of traces such as that in (a) performed on 20 emitters collecting at 540nm.

These findings are remarkably similar to previous observations by LeBlanc *et al.* on CdSe/ZnS core-shell QDs deposited on a gold surface. These authors reported a two-fold increase in dim state accompanied by a shorter lifetime and a two-fold decrease in bright state intensity.[21] The enhanced dim state emission was attributed to an increase in the radiative rate of the bi-exciton state accompanied by a decrease in the Auger recombination rate.

Consistent with the proposed plasmonic enhancement of the bi-excitonic emission, there is a significant increase in $g^{(2)}(0)$) relative to the side bands on the Au-coated substrate *versus* that on glass (Figure 7 and Table 1). In addition, Si NPs on the plasmonic substrates exhibit shorter emission decays (Table 1, Figure 7c) and consequently narrower $g^{(2)}(\tau)$ peaks (Figure 7b) than on glass. Taken as a whole, a plasmonic enhancement of the collective or bi-excitonic (dim) emission that underlies the bright yellow CT emission is observed.

Measurements of decay kinetics are helpful to better understand the mechanisms by which the Au surface impacts the emission yields of the CT and bi-exciton states. Below assignments of the

various decay components on glass are proposed using solution-phase results as reference. Next, the effects on the dynamics of plasmonic interactions are described.

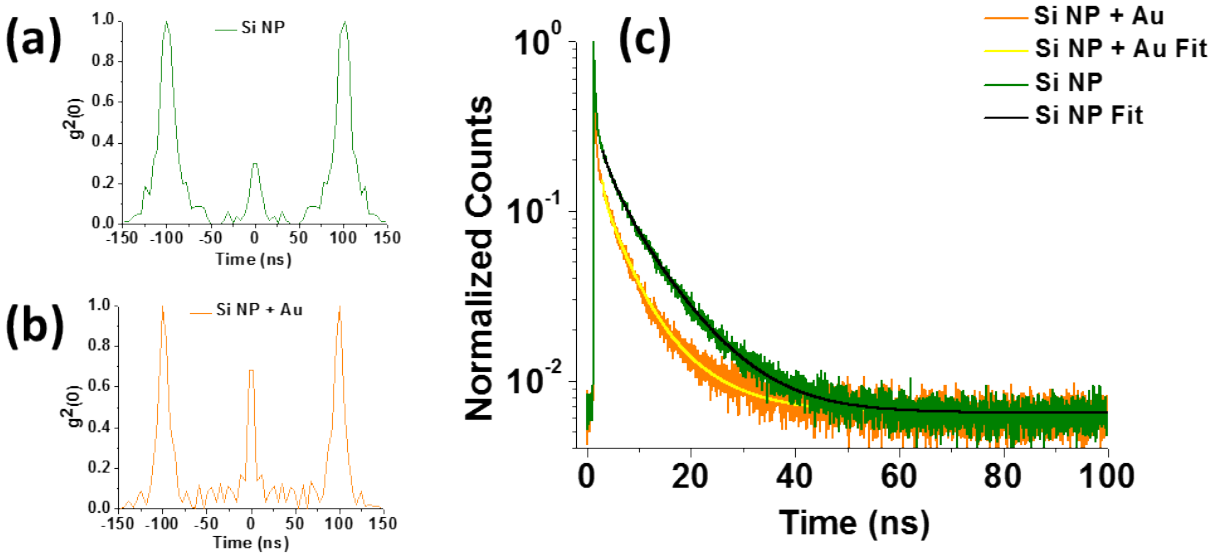

Figure 7. Anti-bunching signal from single Si NP particles on (a) glass and (b) Au film. The average $g^2(0)$ values from 20 particles each are 0.22 ± 0.02 and 0.72 ± 0.07 on glass and Au film, respectively. (c) Lifetimes of the total emission collected from a single Si NP and Si NP + Au film. In both (a) and (b), emission was collected in the range 540nm ± 25nm.

The assignment of these decay processes in solution is relatively straightforward. As the ~3ns component dominates in the yellow emission whereas the ~10ns component dominates in the red emission, these are assigned, respectively, to the ligand-derived CT state and a collective or bi-excitonic state derived from the Si core as discussed earlier. The latter assignment is motivated by the observation of photon-bunching in the red emission as discussed above. It differs from that proposed by Kůsová *et al.*[31] in that we expect the red emission in solution to arise from a neutral rather than a charged (trionic) state. We reason that, given the relatively short lifetime of these Si NPs (≤10ns), the formation of charged states is less likely in solution than in the solid state. The proposed mechanisms for charged trion formation in Si nanocrystals are multiple excitation events and/or transfer of an electron to or from the surrounding matrix.[31] This is less probable in solution

given that there is constant exchange of the sample in and out of the laser beam. Finally, the ~1ns decay component is assignable to non-radiative relaxation processes.

The picture is somewhat different for Si NPs in the solid state. Because lifetime data in the solid could only be measured at the emission peak (540nm) due to low signal in the red region, the properties of the dim and bright emission will be compared. The sub-ns components (IRF limited and ~1ns lifetimes) are assigned to non-radiative decay of the bi-excitonic or collective state because these only contribute substantially to the decay of the dim emission (Figure 4b and Table 1). This is consistent with the solution-phase results described earlier and with previous studies on semiconductor QDs.[59–61] Surprisingly, the ~10ns component in the solid is prominent in both the bright and dim states at 540nm whereas it is not prominent at 540nm in solution (Figure 8 and Table 1). We conjecture that this is due to an inability to fully separate the CT and bi-excitonic emission due to the spectral overlap (Figure 1b). We attempted to test this hypothesis by further subdividing the bright state emission (above 80 counts/10ms) into an intermediate bright state (300 counts/10ms – 80 counts/10ms) and highly bright state (above 300 counts/10ms) but found that the emission at all three brightness levels showed a significant ~10 ns component (ESI Figures S6 and S7 and Table 1). In contrast, the ~1ns component is quite prominent in the dim emission decays and absent in that of the bright emission which supports our assertion that the bright and dim emission arises from the relaxation of two distinct electronic states. Nonetheless, given the complexity of the observed emission decays, anti-bunching measurements (Figure 4c) are a more unambiguous probe of bi-excitonic or collective character for these systems.

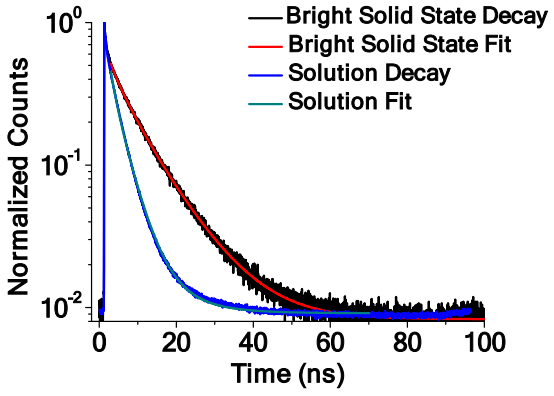

Figure 8. Comparison of emission decays between bright emission in the solid state and in solution measured at 540nm ± 25nm.

The rate of emission decay significantly increases in Si NPs on a plasmonic Au relative on that on glass (Figure 7c). In fact, the overall emission decay on gold is essentially identical to that of the dim state on glass (ESI Figure S8). This is due to fast quenching of the bright CT emission by the gold substrate that leaves the dim (bi-excitonic) emission relatively unaffected. A clearer picture of the effects of gold on the CT and bi-excitonic dynamics is obtained by applying intensity thresholds to separate the emission into bright and dim components as was done earlier. On gold, the decay rate of the dim state is significantly faster than that of the bright state (ESI Figure S9 and Table 1), supporting the model that these two emissions originate from different electronic states. Notably, the bright state emission decay is similar on gold and glass (ESI Figure S10 and Table 1), despite the substantial quenching observed in the intensity traces (Figure 6). This suggests that the CT state is statically quenched, meaning that the quenching process is much faster than the excited state lifetime and is therefore unresolvable. Likely mechanisms include very short range non-radiative energy transfer and potentially electron/charge transfer between the Si NP and the metal surface. In contrast, the dim state on gold exhibits a predominantly IRF limited decay profile (ESI Figure S9 and Table 1) that is significantly faster than that on glass even though its emission is enhanced on the metal surface (Figures 6, 7 and S11). These two factors in combination indicate that the plasmonic enhancement of the radiative rate of this state exceeds that of any intrinsic or gold-induced non-radiative decay effects.

Conclusions

In summary, anti-bunching measurements on ligand-modified Si NPs provide evidence for the contributions of both single- and bi-excitonic states to their emission properties. The dominant emission, derived from CT states on the particle surface, exhibits blinking and anti-bunching which is consistent with single-quantum-state character. Weaker emission that exhibits characteristics of a bi-excitonic state is also observed, predominantly in the red. This is argued to derive from the Si particle core. Furthermore, plasmonic interactions are shown to preferentially enhance the bi-excitonic core emission of these Si NPs but lead to increased quenching of the CT state. Together,

measurements of photon anti-bunching and of plasmonic effects on the emission properties are shown to provide a relatively unambiguous method for assigning single- versus bi-excitonic character, particularly in systems for which the emission from these states have significant wavelength overlap.

Conflicts of Interest

There are no conflicts to declare.

Acknowledgement

L. A. P. acknowledges NSF-CHE 1363050 for support of the instrumentation used in this work. R.J. is grateful for the financial support from the Air Force Office of Scientific Research under AFOSR Award No. FA9550-15-1- 9999 (FA9550-15-1-0154) and the Camille Dreyfus Teacher Scholar Awards Program. Dr. Gizelle Sherwood is thanked for assistance with the single-molecule dispersed emission apparatus.

References

1 L. T. Canham, *Appl. Phys. Lett.*, 1990, **57**, 1046–1048.
2 A. G. Cullis and L. T. Canham, *Nature*, 1991, **353**, 335–338.
3 M. Dasog, J. Kehrle, B. Rieger and J. G. C. Veinot, *Angewandte Chemie International Edition*, 2016, **55**, 2322–2339.
4 C. Chiappini, E. De Rosa, J. O. Martinez, X. Liu, J. Steele, M. M. Stevens and E. Tasciotti, *Nat Mater*, 2015, **14**, 532–539.
5 J.-H. Park, L. Gu, G. von Maltzahn, E. Ruoslahti, S. N. Bhatia and M. J. Sailor, *Nat Mater*, 2009, **8**, 331–336.
6 B. F. P. McVey and R. D. Tilley, *Accounts of Chemical Research*, 2014, **47**, 3045–3051.
7 C. M. Hessel, D. Reid, M. G. Panthani, M. R. Rasch, B. W. Goodfellow, J. Wei, H. Fujii, V. Akhavan and B. A. Korgel, *Chem. Mater.*, 2012, **24**, 393–401.
8 W. L. Wilson, P. F. Szajowski and L. E. Brus, *Science*, 1993, **262**, 1242–1244.
9 J. D. Holmes, K. J. Ziegler, R. C. Doty, L. E. Pell, K. P. Johnston and B. A. Korgel, *J. Am. Chem. Soc.*, 2001, **123**, 3743–3748.
10 D. Jurbergs, E. Rogojina, L. Mangolini and U. Kortshagen, *Appl. Phys. Lett.*, 2006, **88**, 233116.
11 Q. Li, Y. He, J. Chang, L. Wang, H. Chen, Y.-W. Tan, H. Wang and Z. Shao, *J. Am. Chem. Soc.*, 2013, **135**, 14924–14927.
12 Q. Li, T.-Y. Luo, M. Zhou, H. Abroshan, J. Huang, H. J. Kim, N. L. Rosi, Z. Shao and R. Jin, *ACS Nano*, 2016, **10**, 8385–8393.
13 L. Wang, Q. Li, H.-Y. Wang, J.-C. Huang, R. Zhang, Q.-D. Chen, H.-L. Xu, W. Han, Z.-Z. Shao and H.-B. Sun, *Light Sci Appl*, 2015, **4**, e245.
14 W. Y. So, Q. Li, C. M. Legaspi, B. Redler, K. M. Koe, R. Jin and L. A. Peteanu, *ACS Nano*, 2018, **12**, 7232–7238.
15 Y. Zhong, F. Peng, X. Wei, Y. Zhou, J. Wang, X. Jiang, Y. Su, S. Su, S.-T. Lee and Y. He, *Angew. Chem. Int. Ed.*, 2012, **51**, 8485–8489.
16 M. Dasog, Z. Yang, S. Regli, T. M. Atkins, A. Faramus, M. P. Singh, E. Muthuswamy, S. M. Kauzlarich, R. D. Tilley and J. G. C. Veinot, *ACS Nano*, 2013, **7**, 2676–2685.
17 Y. Zhong, X. Sun, S. Wang, F. Peng, F. Bao, Y. Su, Y. Li, S.-T. Lee and Y. He, *ACS Nano*, 2015, **9**, 5958–5967.
18 Y. Yu, C. E. Rowland, R. D. Schaller and B. A. Korgel, *Langmuir*, 2015, **31**, 6886–6893.
19 R. Sinelnikov, M. Dasog, J. Beamish, A. Meldrum and J. G. C. Veinot, *ACS Photonics*, 2017, **4**, 1920–1929.
20 G. M. Carroll, R. Limpens and N. R. Neale, *Nano Lett.*, 2018, **18**, 3118–3124.
21 S. J. LeBlanc, M. R. McClanahan, M. Jones and P. J. Moyer, *Nano Letters*, 2013, **13**, 1662–1669.
22 S. J. LeBlanc, M. R. McClanahan, T. Moyer, M. Jones and P. J. Moyer, *Journal of Applied Physics*, 2014, **115**, 034306.
23 S. Dey and J. Zhao, *The Journal of Physical Chemistry Letters*, 2016, **7**, 2921–2929.
24 C. T. Yuan, P. Yu, H. C. Ko, J. Huang and J. Tang, *ACS Nano*, 2009, **3**, 3051–3056.

25 B. Ji, E. Giovanelli, B. Habert, P. Spinicelli, M. Nasilowski, X. Xu, N. Lequeux, J.-P. Hugonin, F. Marquier, J.-J. Greffet and B. Dubertret, *Nature Nanotechnology*, 2015, **10**, 170–175.
26 G. A. Blab, S. Oellerich, R. Schumm and T. Schmidt, *Opt. Lett.*, 2004, **29**, 727–729.
27 L. A. Peteanu, G. A. Sherwood, J. H. Werner, A. P. Shreve, T. M. Smith and J. Wildeman, *The Journal of Physical Chemistry C*, 2011, **115**, 15607–15616.
28 J. A. Smyder, A. R. Amori, M. Y. Odoi, H. A. Stern, J. J. Peterson and T. D. Krauss, *Phys. Chem. Chem. Phys.*, 2014, **16**, 25723–25728.
29 D. S. English, L. E. Pell, Z. Yu, P. F. Barbara and B. A. Korgel, *Nano Letters*, 2002, **2**, 681–685.
30 K. Kůsová, O. Cibulka, K. Dohnalová, I. Pelant, J. Valenta, A. Fučíková, K. Žídek, J. Lang, J. Englich, P. Matějka, P. Štěpánek and S. Bakardjieva, *ACS Nano*, 2010, **4**, 4495–4504.
31 K. Kůsová, I. Pelant and J. Valenta, *Light: Science & Applications*, 2015, **4**, e336.
32 J. Martin, F. Cichos, F. Huisken and C. von Borczyskowski, *Nano Letters*, 2008, **8**, 656–660.
33 M. D. Mason, G. M. Credo, K. D. Weston and S. K. Buratto, *Physical Review Letters*, 1998, **80**, 5405–5408.
34 P. Michler, A. Imamoglu, M. D. Mason, P. J. Carson, G. F. Strouse and S. K. Buratto, *Nature*, 2000, **406**, 968–970.
35 G. Nair, J. Zhao and M. G. Bawendi, *Nano Letters*, 2011, **11**, 1136–1140.
36 B. Lounis, H. A. Bechtel, D. Gerion, P. Alivisatos and W. E. Moerner, *Chemical Physics Letters*, 2000, **329**, 399–404.
37 R. H. Brown and R. Q. Twiss, *Nature*, 1956, **177**, 27–29.
38 W. Patrick Ambrose, P. M. Goodwin, J. Enderlein, D. J. Semin, J. C. Martin and R. A. Keller, *Chemical Physics Letters*, 1997, **269**, 365–370.
39 Ü. Mets, J. Widengren and R. Rigler, *Chemical Physics*, 1997, **218**, 191–198.
40 P. Tinnefeld, C. Müller and M. Sauer, *Chemical Physics Letters*, 2001, **345**, 252–258.
41 Y.-S. Park, A. V. Malko, J. Vela, Y. Chen, Y. Ghosh, F. García-Santamaría, J. A. Hollingsworth, V. I. Klimov and H. Htoon, *Phys. Rev. Lett.*, 2011, **106**, 187401.
42 B. D. Mangum, Y. Ghosh, J. A. Hollingsworth and H. Htoon, *Opt. Express*, 2013, **21**, 7419–7426.
43 P. F. Barbara, A. J. Gesquiere, S.-J. Park and Y. J. Lee, *Accounts of Chemical Research*, 2005, **38**, 602–610.
44 P. Kumar, T.-H. Lee, A. Mehta, B. G. Sumpter, R. M. Dickson and M. D. Barnes, *J. Am. Chem. Soc.*, 2004, **126**, 3376–3377.
45 C. Wu, B. Bull, C. Szymanski, K. Christensen and J. McNeill, *ACS Nano*, 2008, **2**, 2415–2423.
46 T. Stangl, P. Wilhelm, K. Remmerssen, S. Höger, J. Vogelsang and J. M. Lupton, *Proceedings of the National Academy of Sciences*, 2015, **112**, E5560–E5566.
47 B. Fisher, J. M. Caruge, D. Zehnder and M. Bawendi, *Phys. Rev. Lett.*, 2005, **94**, 087403.
48 S. Dey, Y. Zhou, Y. Sun, J. A. Jenkins, D. Kriz, S. L. Suib, O. Chen, S. Zou and J. Zhao, *Nanoscale*, 2018, **10**, 1038–1046.
49 S. Masuo, T. Vosch, M. Cotlet, P. Tinnefeld, S. Habuchi, T. D. M. Bell, I. Oesterling, D. Beljonne, B. Champagne, K. Müllen, M. Sauer, J. Hofkens and F. C. De Schryver, *J. Phys. Chem. B*, 2004, **108**, 16686–16696.

50 Z. Yang, G. B. De los Reyes, L. V. Titova, I. Sychugov, M. Dasog, J. Linnros, F. A. Hegmann and J. G. C. Veinot, *ACS Photonics*, 2015, **2**, 595–605.
51 K. Dohnalová, A. N. Poddubny, A. A. Prokofiev, W. D. de Boer, C. P. Umesh, J. M. Paulusse, H. Zuilhof and T. Gregorkiewicz, *Light Sci Appl*, 2013, **2**, e47.
52 J. J. Peterson and D. J. Nesbitt, *Nano Lett.*, 2009, **9**, 338–345.
53 F. Pevere, I. Sychugov, F. Sangghaleh, A. Fucikova and J. Linnros, *The Journal of Physical Chemistry C*, 2015, **119**, 7499–7505.
54 F. Sangghaleh, B. Bruhn, T. Schmidt and J. Linnros, *Nanotechnology*, 2013, **24**, 225204.
55 M. C. Beard, K. P. Knutsen, P. Yu, J. M. Luther, Q. Song, W. K. Metzger, R. J. Ellingson and A. J. Nozik, *Nano Letters*, 2007, **7**, 2506–2512.
56 S. Dey, Y. Zhou, X. Tian, J. A. Jenkins, O. Chen, S. Zou and J. Zhao, *Nanoscale*, 2015, **7**, 6851–6858.
57 H.-W. Cheng, C.-T. Yuan, J.-S. Wang, T.-N. Lin, J.-L. Shen, Y.-J. Hung, J. Tang and F.-G. Tseng, *The Journal of Physical Chemistry C*, 2014, **118**, 18126–18132.
58 Y.-S. Park, Y. Ghosh, Y. Chen, A. Piryatinski, P. Xu, N. H. Mack, H.-L. Wang, V. I. Klimov, Jennifer. A. Hollingsworth and H. Htoon, *Phys. Rev. Lett.*, 2013, **110**, 117401.
59 A. L. Efros and D. J. Nesbitt, *Nature Nanotechnology*, 2016, **11**, 661–671.
60 Y.-S. Park, W. K. Bae, J. M. Pietryga and V. I. Klimov, *ACS Nano*, 2014, **8**, 7288–7296.
61 P. P. Jha and P. Guyot-Sionnest, *ACS Nano*, 2009, **3**, 1011–1015.